ONE AND TWO DIMENSIONAL MODELING OF THE BHT-1000

James J. Szabo, Peter. S. Rostler, Seth A. McElhinney, Noah Z. Warner

Busek Co. Inc., 11 Tech Circle, Natick, MA 01760, The United States of America
www.busek.com

Abstract

A 1-kW Hall thruster was numerically modeled using 1-D and 2-D time-dependent methodologies. The 1-D model includes side walls and some 2-D effects, and uses a second-order predictor-corrector scheme. The model is very fast; typical runs take several hours. The 2-D full PIC simulation models a realistic geometry, with wall effects such as ion accommodation and recycling and secondary electron emission. Because the 2-D model resolves oscillations on the order of the plasma frequency, typical runs take several days. Predictions of both models are compared to laboratory data and to each other. Figures of merit include performance predictions and the capture of experimentally observed discharge oscillations. Other areas of interest include plasma parameters such as electron temperature, plasma density, and plasma potential. Agreement of results with each other and with reality is encouraging. Busek is using its modeling tools to refine its thruster designs.

Introduction

This paper describes modeling of the BHT-1000, shown in Figure 1. This thruster was developed for high I_{sp} operation.[1] The discharge cavity diameter is 6.8 cm. The thruster can be configured to run in 1 or 2 stages. This paper concerns the single-stage configuration, diagrammed in Figure 2. The nominal propellant is xenon. The cathode typically floats about 15 V below facility ground.

The magnetic field was designed using the commercial finite element program Maxwell and verified with a Gauss meter. The field is tailored with pole pieces and magnetic shunts to have a focusing geometry for minimal beam divergence, and an increasing magnitude for discharge stability. Maxwell's predictions were used for 1-D and 2-D modeling.

Our goal is to fully integrate numerical models in the thruster design process. Successful models can augment and even supplant some laboratory testing. Just as CFD has advanced the art of chemical rocket design, so can plasma modeling advance electric rocket design. Longer lifetime and greater efficiency may be thus obtained.

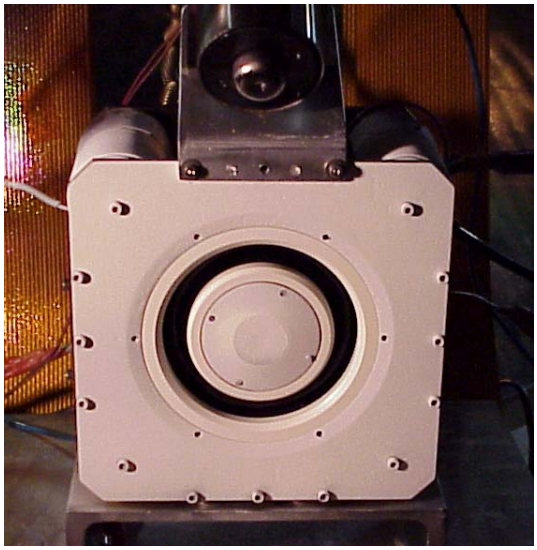

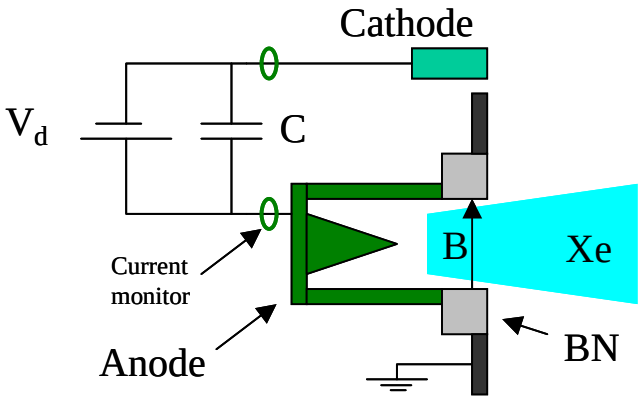

Figure 1. Left: BHT-1000 Hall effect thruster in September/October 2002.

Figure 2. Right: The nominal (single stage) discharge chamber of the BHT-1000 with a simple electrical diagram. The discharge potential is applied between the floating cathode potential and the anode. A capacitor is connected in parallel.

The BHT-1000 has been characterized in our facilities. Figure 3 shows the nominal specific impulse (I_{sp}) with $\dot{m} = 2.5$ mg/s of Xe flowing through the anode. Error bars for these data are several percent. Figure 3 also plots the thrust efficiency, $\eta_t = T^2/2\dot{m}I_d V_d$, and utilization efficiency $\eta_u = \dot{m}_i/\dot{m}_{total}$, for a range of voltages at the same flow rate. To estimate η_u, we assume that acceleration efficiency, $\eta_a = M < v_i >^2 /2eV_d$, is a function (plotted in Figure 3) of the discharge potential, V_d. Some variation arises from adjustments to the magnetic field intended to minimize current and/or maximize thrust. At $\dot{m} = 2.5$ mg/s and discharge voltage V_d=1000 volts, the single-stage BHT-1000 achieves I_{sp} ~ 3000 sec with a thrust efficiency of about η_t =50%. Higher flow rates yield slightly better performance.

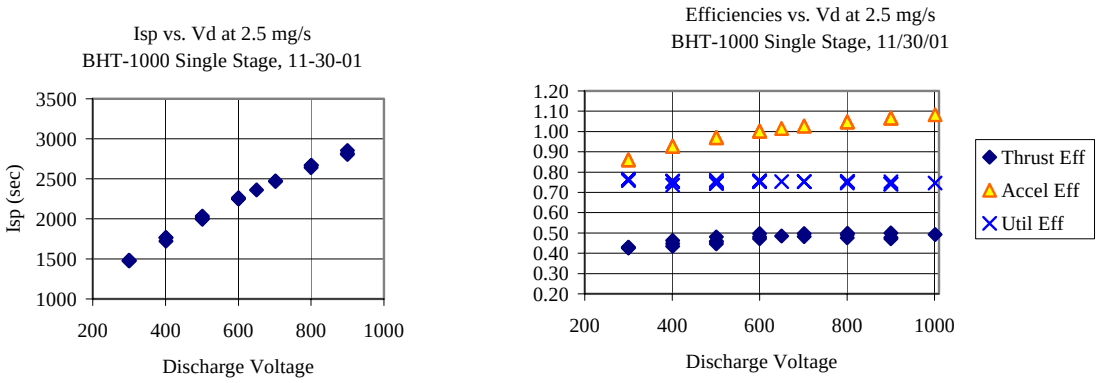

Figure 3. Typical performance of the BHT-1000 thruster in its nominal configuration with $\dot{m} = 2.50$ mg/s.

To measure discharge oscillations, Pearson Electronics Model 110 current monitors (signal strength of .1 V/Amp) were placed around the anode and cathode leads, as shown in Figure 2. The thruster was then run at nominal operating conditions. Figure 4 shows oscilloscope traces obtained with $\dot{m} = 2.5$ mg/s, capacitance C=40 μF, and discharge potentials of V_d=300 V and 600 V. In both cases, the current through the four outer solenoids is I_o=8 Amps, and the current through the inner solenoid is I_i=11.1 Amps. The field should, therefore, be close to that used for the 1-D and 2-D simulations. The 300 Volt plot is interesting in that the anode current appears to have a characteristic frequency of 20 kHz, while the cathode current oscillates at 47 kHz. The amplitude is about +/- .1 Amps. The 600 Volt plot shows the cathode and anode oscillating together at 42 kHz with an amplitude of about +/- .5 Amps.

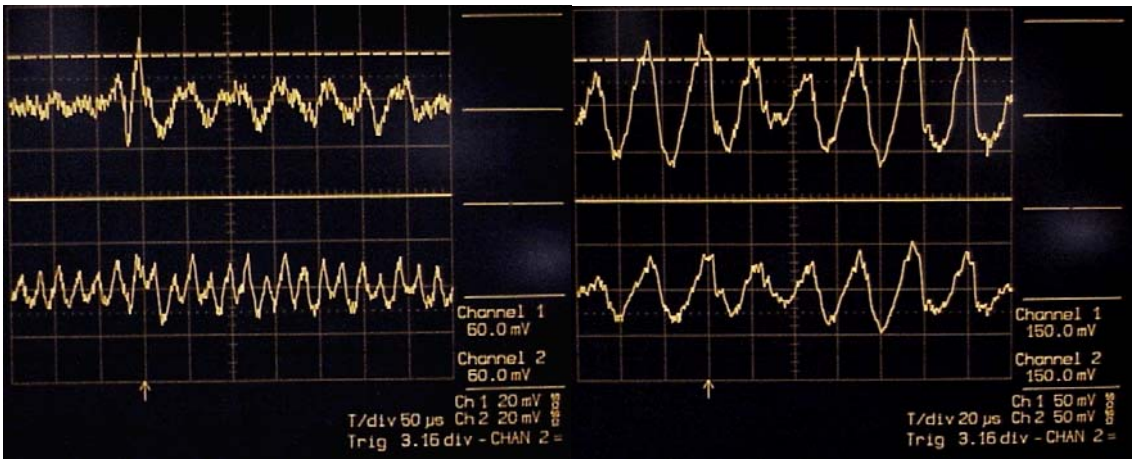

Figure 4. Oscilloscope traces. Top trace is anode current. Bottom trace is cathode current. Conditions: $\dot{m} = 2.5$ mg/s; C= 40 μF ; I_o=8 A; I_i=4 11.1. Left: V_d=300 V. The vertical scale is .2 Amps per division. Right: V_d=600 V. The vertical scale is .5 Amps per division.

Magnetic Field Modeling

Numerical results generated with two different Maxwell B-field predictions are presented in this paper. The field dated 2/19/03, shown in Figure 5, is slightly smoother and more accurate than the field dated 2/13/02, used for previously reported BHT-1000 simulations. Unless otherwise indicated, numerical predictions reported in this paper use the newer field.

To accurately model the discharge, we need to ensure that our B-field agrees with reality. In August, 2002, the B-field profile was measured with a Gauss meter. The left side of Figure 5 compares the measured |B| along a line at R=34.9 mm and Maxwell predictions dated 2/19/03. The Z axis represents the axial direction. Good agreement is obtained in shape, but a factor of .92 was applied to the predicted |B| in order to match the measured |B|. The right side of Figure 5 shows the streamlines and magnitude contours used in the 2-D simulation. Again, the .92 factor was applied. Note the "magnetic lens" shape obtained via magnetic shunts.

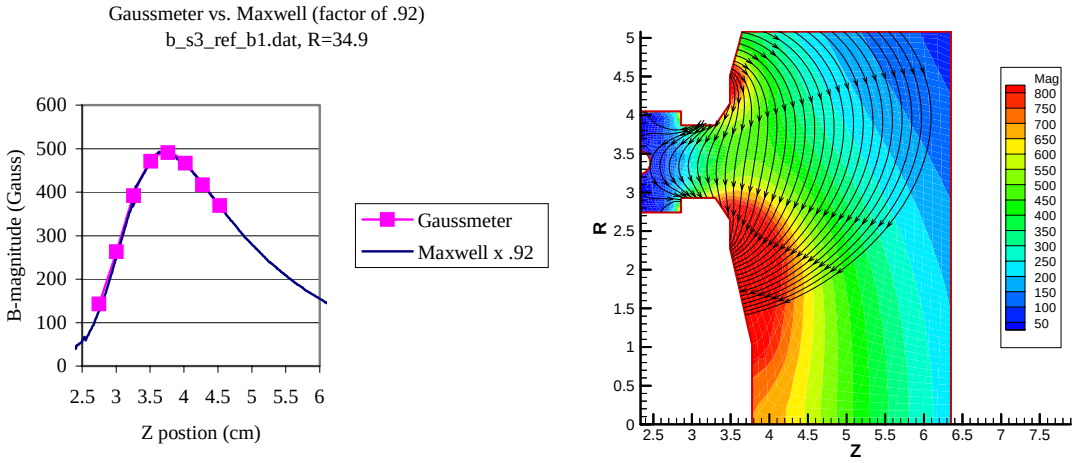

Figure 5. Left: Measurements of |B| are compared to Maxwell results interpolated to a line at R=34.9 mm, close to the center of the channel. A factor of 0.92 is applied to the Maxwell predictions. Right: The magnetic field used for modeling. Shown are magnetic streamlines and contours of |B|. The magnitude is .92 times the original Maxwell prediction, but the shape is the same.

Since the B-field was mapped in August 2002, the inner solenoid was replaced. Subsequent (but cursory) azimuthally distributed measurements of |B| showed a small but measurable increase in magnitude. This suggests some turns on the inner coil may have been shorted during the August mapping. Changes in B-field magnitude have been observed to change the oscillation frequency by several kHz.

1-Dimensional Modeling

Our 1-D time-dependent model has been described previously.[2] This model includes side walls and other 2-D effects. In particular, it includes the loss of ions to the side walls of the channel, which reduce efficiency and limit lifetime by eroding (sputtering) the wall material. Recent changes include implementation of a second-order predictor-corrector scheme.

The 1-D model was derived from 3-D equations by assuming azimuthal uniformity (except for the effect of non-uniformities on the Hall parameter) and assuming that the radial velocity of each species is a uniform expansion, $u_x^+ = 2v_s^+ x/W$ and that the radial density profile is Gaussian, $n^+(x,z,t) = n^+(z,t)\ exp\ (-2x^2/W^2)$, where x is the radial coordinate, $W(z)$ is the channel width, the walls are at $x = \pm W/2$, and v_s^+ is the ion sound speed, $\sqrt{(n^+kT_e + p^+)/n^+M}$. Used in the 3-D equations, this approximation leaves only a few small terms that have to be disregarded to obtain a description that depends only on the axial coordinate z and the time t.

Besides side-wall losses, this 1-D model retains a 2-D channel geometry, described by $W(z)$ and a 2-D magnetic field described by $B(z)$, by the angle $\psi(z)$ between a normal to B and the wall, and by $A(z)$, the ratio of the area of a flux tube at the wall to its area at the mid-plane of the channel. Figure 6 shows the

channel geometry and the coordinates. As implied by the inclusion of the ion pressure, $p^+ = n^+ k T^+$ in the sound speed, our model also includes ion temperatures, T^+ and T^{++}. These were retained because they affect the flow of ions into the walls.

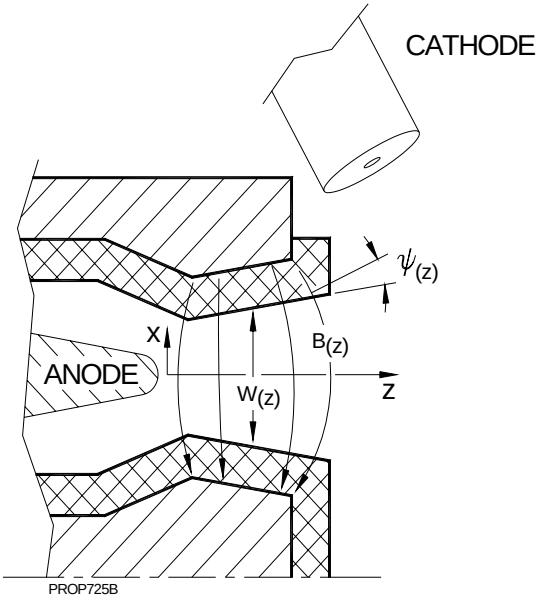

Figure 6. Hall thruster geometry and coordinates of the 1-D model.

There are four species modeled: neutral xenon atoms, singly and doubly charged xenon ions and, of course, the electrons. The result is a description of the discharge by eight variables, the neutral, singly-ionized and doubly-ionized xenon densities, $n_0(z,t)$, $n^+(z,t)$ and $n^{++}(z,t)$; the ion velocities, $u_z^+(z,t)$ and $u_z^{++}(z,t)$; the electron temperature, $T_e(z,t)$ and, finally, the ion temperatures $T^+(z,t)$ and $T^{++}(z,t)$. The neutral velocity, $v_0(z,t)$, the electron density $n_e(z,t)$, the electron drift velocity, $v_e(z,t)$, and the electric field $E_z(z,t)$ are just functions of these eight primary variables.

The time evolution of the system is described by eight first-order equations. Xe, Xe^+, and Xe^{2+} densities obey continuity equations. The electron density is determined by quasineutrality. Xe^+ and Xe^{2+} accelerations obey momentum (force) equations including electric forces, pressure gradients, and ionization rates. The electron temperature is determined by heat balance. In contrast to earlier work,[2] the equation is now being solved exactly, without an artificially increased heat capacity. Xe^+ and Xe^{2+} temperatures are also calculated via energy equations. Solved algebraically, the eight equations give time derivatives at each point as functions of the variables at the same and nearby points. Stepped numerically, they predict the dynamics of the discharge.

Logically, the calculation starts knowing the discharge current, obtained from an external circuit. Then, we calculate E and v_e. The electric field is determined by an Ohm's law equation which includes an anomalous Hall parameter. The electron velocity is that needed to carry the discharge current. The collision and ionization rates are functions of the electron temperature based on data. These variables are then used in the continuity, momentum, and energy equations previously mentioned to calculate at every point the time derivatives of the eight primary variables. The neutral gas velocity is given by simple diffusion with a constant neutral temperature. So the treatment of the electrons and the neutrals is fairly simple, but the ion dynamics and the discharge kinetics are analyzed in more detail.

A predictor-corrector code has been written to solve these equations. It uses a fixed grid and a variable time step. Gradients are calculated to third order on the upstream side. Gas enters through the anode from a reservoir that is replenished at the gas feed rate. The entering gas is assumed to be a few percent ionized. On each step, the code starts knowing the discharge current and calculates the E-field and hence the voltage, which is then used in the equations for the external circuit to calculate the current for the next time step. This code is now running stably and producing solutions to the model.

Although our 1-D model was derived from first principles as much as possible, a few adjustable parameters were unavoidable. Besides the neutral gas temperature, the anomalous Hall parameter (to account for transport by plasma fluctuations) and the degree of pre-ionization (to account for radiative transport or a weak discharge behind the anode), the code also includes a velocity reduction factor that

multiplies the transverse velocity with which the ions flow into the side walls. Ions acquire temperature in the axial direction, by being made at different locations with different potentials. The derivation assumes this temperature becomes isotropic, which almost certainly gives too pessimistic an estimate of the side wall losses, so these are reduced by an added factor.

The model also includes side wall conductivity, to account for current flowing through sheaths or on insulator surfaces. Without this, one gets an "opening switch" effect where the ion density drops at some location, producing a stronger electric field to carry the current there, which accelerates ions out of the region even faster, reducing the density further. If Hall thrusters did that, it would be very useful, but they do not, presumably because current can flow along the walls. There is also some uncertainty in discharge length, that is, in the distance from the anode to the field lines that are electrically tied to the cathode. The comparisons below are based upon our first estimates of these several parameters.

source	Quasi 1D
date	3/6/2003
B-field	**2/19/2003**
Hall	200
Vd (V)	285
Id (A)	3.1
dm/dt (mg/s)	2.50
Thrust (mN)	35
Isp (sec)	1510
n t	0.31
nu ion (kHz)	14
utilization	0.98

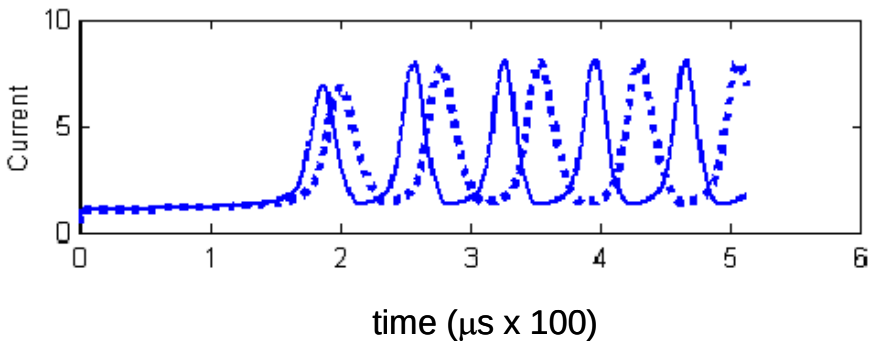

Figure 7. 1-D model predictions of discharge current for anode potential of 285 Volts. Oscillation frequency is about 14 kHz. C=80 μF assumed. Solid line: 70 grid points. Dotted line: 20 grid points.

Performance predictions of the 1-D model are found in the table in Figure 7. For comparison, experimental performance and predictions of the 2-D model are round in Table 1, found in the next section. With the parameters used in this run, the 1-D model underestimates energy efficiency and overestimates gas utilization, although both are of the right order. The predicted I_{sp} agrees well with our thrust measurements.

The current trace in Figure 7 is the 1-D model prediction for a 500 μs discharge at 285 volts. The frequency of oscillation is about 14 kHz. In runs at higher voltage, the predicted oscillation frequency decreased slightly and the current peaks became sharper and of larger amplitude.

The speed of the 1-D code depends on the desired precision. With a coarser grid, it runs much faster, as illustrated by Figure 7. There the solid line is a run with 70 grid points. It took six hours. The dotted line is the same case with 20 points. That took six minutes. There's some frequency error, but to survey many cases quickly, this would be good enough.

Spatial profiles of the *E* field and electron density at four evenly spaced times during one cycle of the oscillation (low, rising, peak and falling current) are shown in Figure 8, which was generated with the finer grid. There the anode is on the left and the cathode on the right. The time labels refer to Figure 7. The vertical lines, present for orientation only, represent (left to right) the beginning of the boron nitride discharge channel walls (Z=2.86), the beginning of the chamfer (Z=3.30), and the end of the walls (Z=3.49). As can be seen, the predicted electron density varies by about a factor of thirty during the cycle. The neutral density (not shown) only drops by about 25% during the cycle. When the current and ionization are low, the electric field is relatively uniform, but at the time of peak current, when the ionization is more than an order of magnitude higher, the electric field almost vanishes near the anode and becomes much stronger near the output (cathode) end of the thruster.

As further 1-D calculations are compared to data and to the predictions of the 2-D code, it should be possible to better determine some of these parameters. The 2-D code shows the ion temperature anisotropy, the location of the field lines tied to cathode voltage and the current flowing through the sheaths along the walls, which can then be fed back into the simple 1-D description. Comparison with data may tell us what anomalous Hall parameter, what neutral gas temperature, and what degree of pre-ionization to assume. That process of fine-tuning is still at an early stage, but the agreement between the two codes and the data that we are already seeing is close enough to be encouraging.

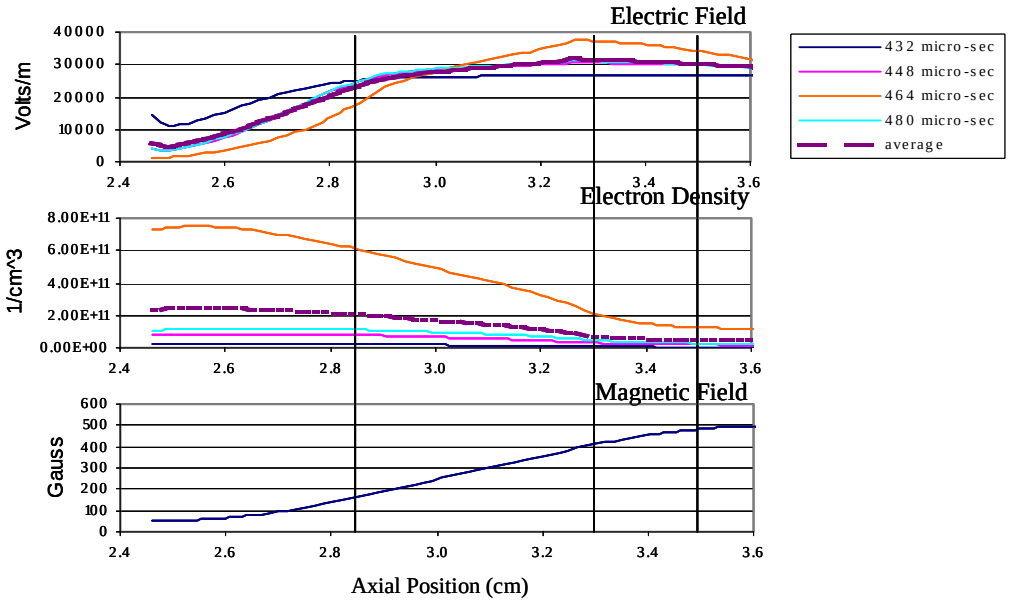

Figure 8. 1-D model predictions of (top to bottom) E-field (V/m) and electron density (1/cc). Also shown is |B| (Gauss) along the centerline, which was used for the calculations. Shown are outputs at 4 points in the ionization oscillation cycle. Averages are also shown on the E-field and density plots.

2-Dimensional Modeling

Our 2-D full PIC model contains doubly charged ions, excitation, charge exchange and other collisions, and a realistic geometry which includes dielectric walls and secondary electron emission. By using an artificial mass ratio and artificial permittivity, the full PIC code is able to capture oscillations on the scale of the electron plasma frequency. Typical runs take several days. This model has been well described in previous publications.[3]

The most significant recent change to the code is a revised ion accommodation coefficient at solid surfaces. As before, we assume full accommodation of ion momentum (diffuse reflection), and partial accommodation in energy. However, previous simulations assumed a recycle neutral retained 50% of its parent ion's kinetic energy, whatever that was. Current simulations assume an energy accommodation coefficient of $\alpha = 60\%$ at energies less than 140 eV, $\alpha = 77\%$ at energies greater than 400 eV, and a linear fit between the endpoints at energies in between. These values are based upon experimental measurements of Xe accommodation on BN by RIAME and MAI.[4]

The 2-D simulation was run with the as-built BHT-1000 geometry and the Maxwell generated B-field with a factor of 0.92 applied to the magnitude. Simulations at discharge potentials of 300 and 600 volts are described below. An artificial mass ratio of M/M'=2500 was assumed, which means M/m~96, where M is the ion mass and m is the electron mass. Various scaling factors are used to produce physical results. Stochastic Bohm type diffusion was added with a proportionality coefficient of 1/200B, as opposed to the classical value of 1/16B. That is, the anomalous Hall parameter is 200. Free space permittivity is typically increased by a factor of 400, which lengthens the Debye length by a factor of γ=20, allowing a coarser grid, and decreases the plasma frequency by a factor of γ=20, allowing a longer time-step. The run time on an AMD Athlon powered PC for a single case with M/m~96 and γ=20 is several days.

Table 1 compares actual performance against predictions at both V_d=300 V (case "A") and V_d=600 V (case "B"), both of which use the more realistic B-field, dated 2/19/03, and the revised accommodation coefficient. Since the cathode is assumed to float at –15 V, a discharge potential of 300 V means an anode potential of 285 V. Predictions are time averaged over one or several ionization oscillations. In general, I_{sp} predictions are good, but the code consistently underestimates the discharge current by half an Amp. The ionization oscillation frequency is also under-predicted, although the relative magnitude of the oscillations is more or less correct. Oscillations will be discussed more below. Table 1 also contains predictions for an older, less realistic B-field, dated 2/13/02. These will also be discussed.

source	"Case A"	Test	"Case B"	Test	PIC	PIC
date	2/26/2003	Typical **	2/25/2003	11/30/01	6/17/2002	12/7/2002
B-field	**2/19/2003**	-	**2/19/2003**	-	**2/13/02**	**2/13/02**
M/M'	2500	-	2500	-	2500	2500
gamma	20	-	20	-	**20**	**10**
Hall	200	-	200	-	200	200
Vd (V)	**300**	**300**	**600**	**600**	300	300
Id (A)	1.50	1.96	1.63	2.07	1.54	1.69
dm/dt (mg/s)	2.47	2.43	2.5	2.50	2.51	2.52
Thrust (mN)	34.8	35.2	50.3	55.5	35.3	35.0
Isp (sec)	1420	1472	2050	2264	1441	1430
n t	0.54	0.43	0.53	0.5	0.54	0.49
nu ion (kHz)	17	45 (typ)	29	42 (typ)	14	15

Table 1. Time averaged 2-D full PIC predictions vs. measured performance. The code under-predicts I_d. More realistic sheath structures increase I_d prediction, but require much longer run-times. Factor dm/dt is the mean particle flux exiting the simulation during the period of time averaging. ** average of several data points

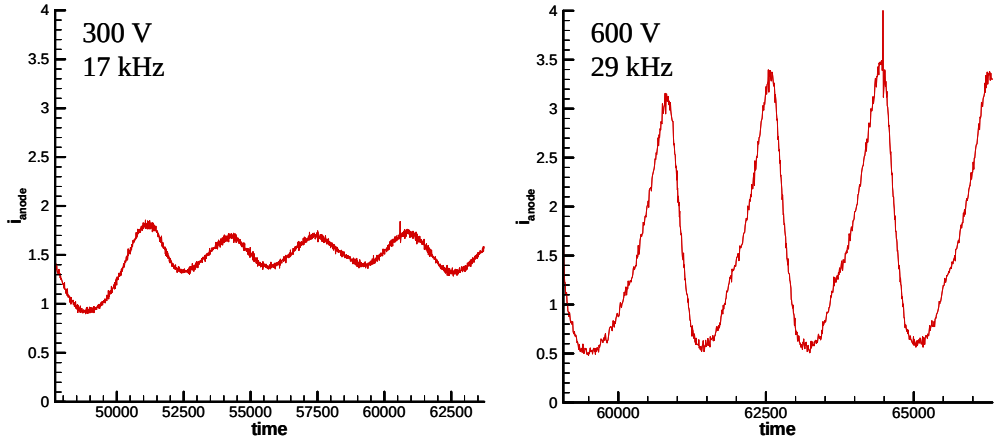

Figure 9. Left: Case A. Anode current oscillations for 300 V discharge, new B-field, γ=20. Right: Case B. 600 V discharge.

Figure 9 plots the discharge current predicted for cases A and B. The 600 V oscillations are several times larger in magnitude than the 300 V oscillations. The same trend was observed experimentally in Figure 4. The frequency of case A (17 kHz) is only about a third of the observed 300 V cathode oscillation frequency (47 kHz), but of the same order. The case A oscillation is closer to the apparent 20 kHz anode oscillation in Figure 4, but the correlation may be spurious. The case B oscillation (29 kHz) is similar to the observed 600 V oscillation (42 kHz).

Figure 10 plots contours of time-averaged electron density for cases A and B. The period of averaging is one numerical oscillation cycle. Also shown are streamlines intersecting Langmuir probes inserted through the walls of the discharge cavity. The most notable change with higher voltage is that the area of peak density moves closer to the anode. The length ($L=\Delta Z$) of the discharge in the 300 V simulation is $L \approx 1$ cm, while the more compact discharge of the 600 V simulation is $L \approx .5$ cm wide.

The density plot allows us to predict the ionization oscillation frequency, which theory[5] says should follow the formula $\varpi = 2\pi f = \sqrt{V_i V_n}/L$. Here, f is the frequency, V_i and V_n are the ion and neutral bulk velocities in the acceleration zone, and L is the axial length of the acceleration zone. Results for case A include velocities near the discharge center of $V_i \approx 5 \times 10^5$ cm/s and $V_n \approx 2 \times 10^4$cm/s. With $L \approx 1$ cm, the formula predicts f=16 kHz, very close to the oscillation plotted in Figure 9. Results for case B are also close. Bulk velocities are $V_i \approx 3 \times 105$ cm/s and $V_n \approx 3 \times 10^4$cm/s. With $L \approx .5$ cm, the formula then predicts f=30 kHz. Thus, within the context of the simulation, the ionization oscillations follow theory.

Figure 11 plots contours of time-averaged electric potential for cases A and B. The plots are very similar except that the contour magnitudes are twice as large for the 600 Volt discharge.

Figure 12 plots contours of time averaged electron temperature for cases A and B. The 300 V simulation predicts a peak of $T_e \approx 20$ eV, while the 600 V simulation predicts a peak of $T_e \approx 45$ eV. The prediction of increasing peak T_e with discharge voltage has been previously reported.[6]

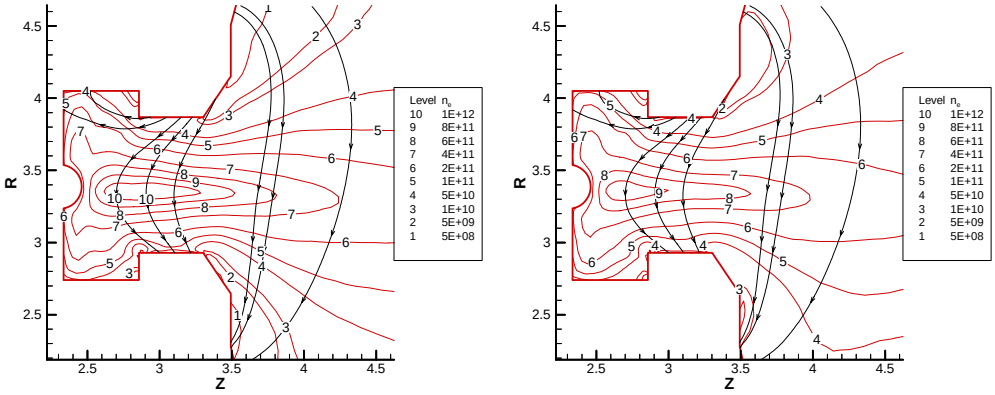

Figure 10. Left: Electron density predictions for 300 Volt discharge at $\dot{m} = 2.5$ mg/s. Right: Predictions for 600 Volt discharge. Time averaged over one ionization oscillation.

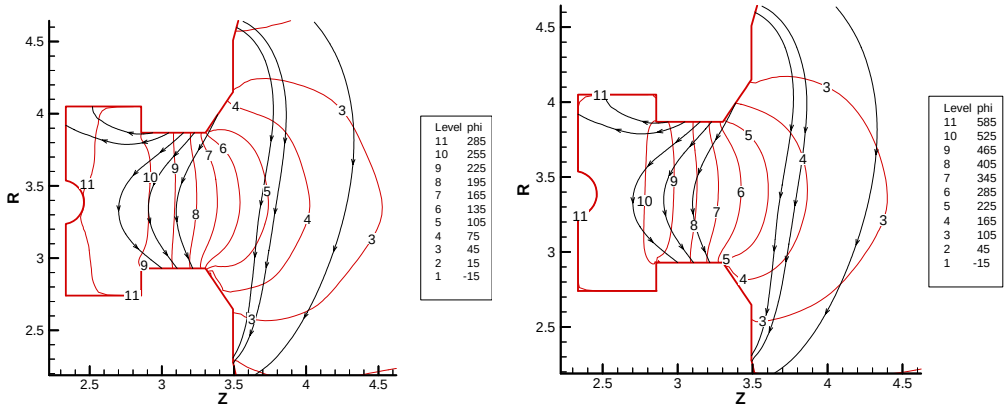

Figure 11. Left: Electric potential predictions for 300 Volt discharge at $\dot{m} = 2.5$ mg/s. Right: Predictions for 600 Volt discharge. Time averaged over one ionization oscillation.

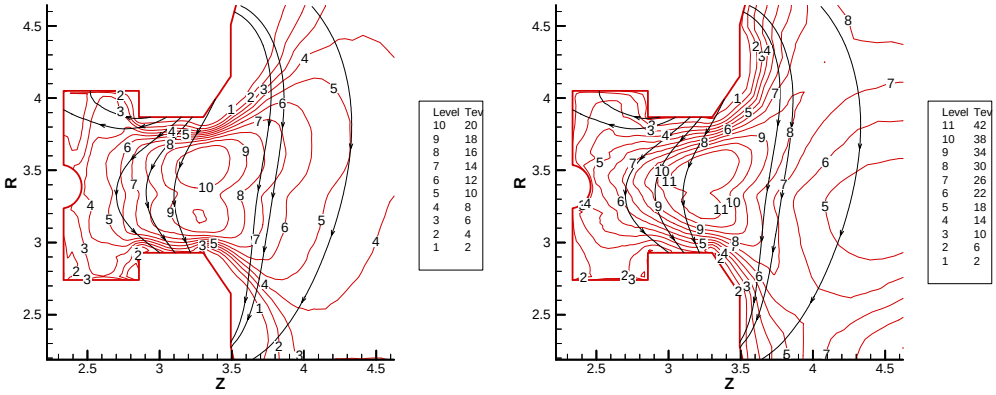

Figure 12. Left: Electron temperature predictions for 300 Volt discharge at $\dot{m} = 2.5$ mg/s. Right: Predictions for 600 Volt discharge. Time averaged over one ionization oscillation.

How does the expanding the Debye length and other sheaths affect the results? With the old (2/13/02) B-field, we ran a complete simulation using a more realistic permittivity (γ=10). This simulation assumed the old ion energy accommodation coefficient of one half. Performance is compared with a γ=20 case using the same B-field and accommodation coefficient in Table 1. Using γ=10 increased the discharge current toward the actual value, which was a positive trend. Traces of I_d for the two cases are plotted in Figure 13. Both cases show a $\approx$15 kHz oscillation, which appears to dampen over time. The γ=10 trace also shows regular high-frequency oscillations at $\approx$125 kHz. Particle moments changed with γ=10, although most only by a little. The discharge seemed to widen in the radial sense, such that contours of n_e assumed a lower aspect ratio ($\Delta Z/\Delta R$), but L remained almost the same. The axial location of the peak n_e only changed by 1mm; it was at 3.15 mm for the coarse grid case, and 3.08 mm for the fine grid case. The electric potential distribution changed just a little; the time-averaged γ=10 potential was about 10 volts higher in the middle of the channel at the beginning of the chamfer. The E-field magnitude at this point was almost the same for both cases. The largest change came in the distribution of electron temperature; the peak moved downstream about 2 mm.

Unfortunately, γ=10 (vs. γ=20) requires a shorter time-step (half as long), a denser grid (4 times as many nodes) and many more particles to maintain good statistics. Together, these factors increase the run time for a single case to several weeks. Hence, γ=20 is a practical limit for engineering purposes.

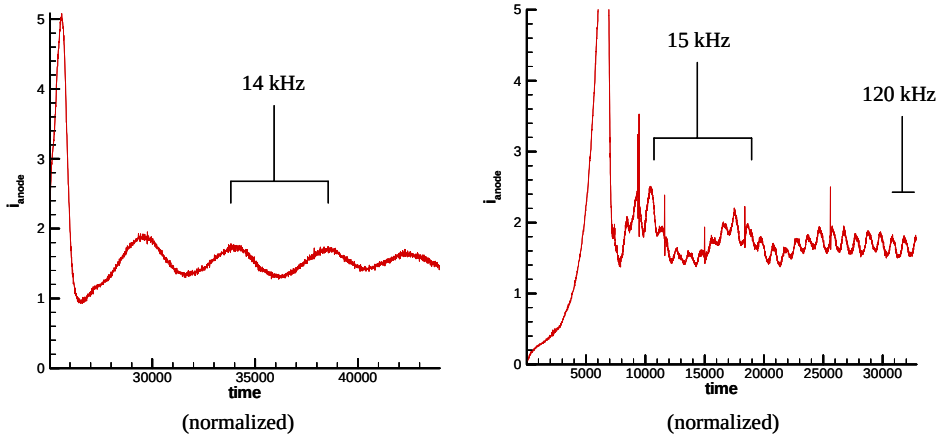

Figure 13. 300 V anode current oscillations for γ=20 (left) and γ=10 (right). Same B-field.

Comparison of 1-D and 2-D Results

To compare with 1-D results as plotted in Figure 8, time averaged 2-D predictions were interpolated to a line along the centerline of the thruster. Figure 14 shows predictions for cases A and B, both of which assume an ion mass ratio of M/m~96. As before, the vertical lines represent the beginning of the BN discharge channel walls, the beginning of the chamfer, and the end of the walls. At 600 V, T_e rises greatly near the upper right hand boundary, but this may be an artifact of the boundary conditions. Also shown in Figure 14 (case D) are time averaged results from a 300 V simulation which uses a more realistic ion mass ratio, M/m~240. Results are close to case A, but the discharge begins closer to the anode, the discharge length L is slightly longer, and the frequency is $\approx$13 kHz. Case D was not averaged over exactly one cycle.

With respect to the 1-D averaged results in Figure 8, the case A peak plasma density is several times higher. The distribution along the axis is, however, similar. The peak T_e is also a few eV higher; boundary conditions in the 1-D model limit temperature to $T_e \approx 16$ eV.

The 1-D model predicts a peak average E-field of $E_z \approx 30{,}000$ V/m, which occurs near the chamfer. The peak time-averaged electric field in case A also occurs near the chamfer. The value along the centerline at that Z is about $E_z \approx 20{,}000$ V/m (as shown in Figure 14) but increases to $E_z > 30{,}000$ V/m outside r=3.75 cm, and inside 3.05 cm (the total width is .94 cm, centered around r=3.4). This is not plotted.

The biggest difference between the 1-D and 2-D predictions is the anode current, which neither code gets right. The 2-D code under-predicts the current by .4 to .5 amps, while the 1-D code over-predicts by the current by about .75 Amps.

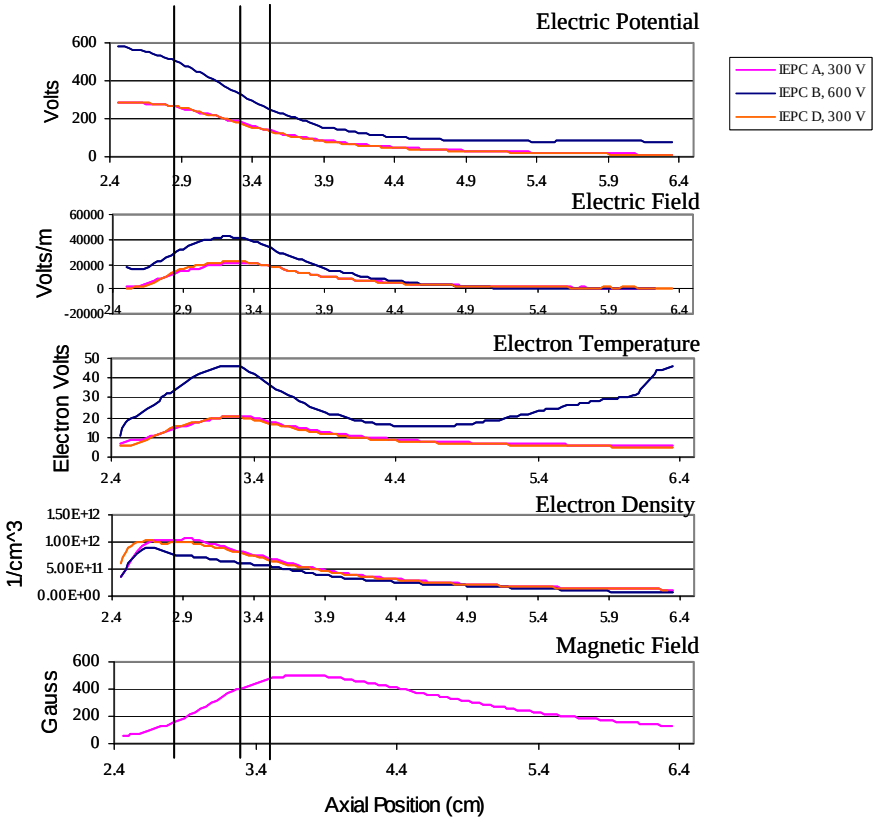

Figure 14. 2-D PIC predictions of centerline quantities for the 300 Volt and 600 V discharges. From top to bottom: Electric potential (V); electric field (V/m); electron temperature (eV); electron density (1/cm^3); magnetic field strength (Gauss); Quantities are time averaged over one ionization oscillation. Vertical bars signify the beginning of the exit ring (Z=2.86), the corner of the chamfer (3.30), and the end of the exit ring (3.49). Case A: V_d =300, M/m=96; Case B: V_d =600, M/m=96; Case D: V_d=300, M/m=240.

Conclusions

Busek's plasma modeling tools are undergoing continuous improvement. The 1-D simulation runs very fast, yielding fairly accurate performance predictions in under an hour. The 2-D simulation is much slower, taking several days to converge, but yields more accurate estimates of plasma parameters. In general, the models compare favorably to each other and to experiments.

References

[1] B. Pote and R. Tedrake, "Performance of a High Specific Impulse Hall Thruster," 2001 International Electric Propulsion Conference, Oct. 15-19, 2001, Pasadena, CA, USA, IEPC-01-35.

[2] P.S.Rostler, "A 1-D Time-Dependent Model of a Hall Thruster with Side Walls," 2001 International Electric Propulsion Conference, Oct. 15-19, 2001, Pasadena, CA, USA, IEPC-01-22.

[3] J. Szabo, M. Martinez-Sanchez, O. Batishchev, "Fully Kinetic Hall Thruster Modeling," 2001 International Electric Propulsion Conference, Oct. 15-19, 2001, Pasadena, CA, USA, IEPC-01-341.

[4] V. Kim, A. Semenov, I. Shkarban, "Investigation of the Accelerated Ions Energy Accommodation Under Their Impingement with Solid Surfaces,", 38th AIAA/ASME/SAE/ASEE Joint Propulsion Conference & Exhibit, 7-10 July 2002, Indianapolis, Indiana, AIAA 2002-4110.

[5] J. M. Fife, M. Martinez-Sanchez, J. Szabo, "A Numerical Study of Low-Frequency Discharge Oscillations in Hall Thrusters," 33rd AIAA/ASME/SAE/ASEE Joint Propulsion Conference, 6-9 July 1997, AIAA-97-3053.

[6] V. Blateau, "PIC simulation of a ceramic-lined Hall-effect thruster," Master's Thesis, MIT Department of Aeronautics and Astronautics, 2002.